Non-permissive SARS-CoV-2 infection in human neurospheres

Carolina da S. G. Pedrosa[1¶], Livia Goto-Silva[1¶], Jairo R. Temerozo[2,3,¶], Ismael C. Gomes[4], Leticia R. Q. Souza[1], Gabriela Vitória[1], Isis M. Ornelas[1], Karina Karmirian[1,4], Mayara A. Mendes[1], Carolina Q. Sacramento[5,6], Natalia Fintelman-Rodrigues[5,6], Vinicius Cardoso Soares[5,7], Suelen da Silva Gomes Dias[5], José Alexandre Salerno[1,4], Teresa Puig-Pijuan[1,8], Julia T. Oliveira[1], Luiz G. H. S. Aragão[1], Thayana C. Q. Torquato[1], Carla Veríssimo[4], Diogo Biagi[9], Estela M. Cruvinel[9], Rafael Dariolli[9], Daniel R. Furtado[1], Helena L. Borges[4], Patrícia T. Bozza[5], Stevens Rehen[1,4,&]*, Thiago Moreno L. Souza[5,6,&]* and Marília Zaluar P. Guimarães[1,4,&]*.

[1] D'Or Institute for Research and Education (IDOR), Rio de Janeiro, RJ, Brazil.

[2] National Institute for Science and Technology on Neuroimmunomodulation (INCT/NIM), Oswaldo Cruz Institute (IOC), Oswaldo Cruz Foundation (Fiocruz), Rio de Janeiro, RJ, Brazil.

[3] Laboratory on Thymus Research, Oswaldo Cruz Institute (IOC), Oswaldo Cruz Foundation (Fiocruz), Rio de Janeiro, RJ, Brazil.

[4] Institute of Biomedical Sciences, Federal University of Rio de Janeiro (UFRJ), Rio de Janeiro, RJ, Brazil.

[5] Immunopharmacology Laboratory, Oswaldo Cruz Institute (IOC), Oswaldo Cruz Foundation (Fiocruz), Rio de Janeiro, RJ, Brazil.

[6] National Institute for Science and Technology on Innovation in Diseases of Neglected Populations (INCT/IDPN), Center for Technological Development in Health (CDTS), Oswaldo Cruz Foundation (Fiocruz), Rio de Janeiro, RJ, Brazil.

[7] Program of Immunology and Inflammation, Federal University of Rio de Janeiro (UFRJ), Rio de Janeiro, RJ, Brazil.

[8] Carlos Chagas Filho Institute of Biophysics, Federal University of Rio de Janeiro (UFRJ), Rio de Janeiro, RJ, Brazil.

[9] Pluricell Biotech, São Paulo, SP, Brazil.

[¶] These authors contributed equally to this work

[&] These authors also contributed equally to this work.

* Corresponding authors

Email: srehen@lance-ufrj.org (SR), tmoreno@cdts.fiocruz.br (TMLS) and marilia@lance-ufrj.org (MZPG).

Abstract

Coronavirus disease 2019 (COVID-19) was initially described as a viral infection of the respiratory tract. It is now known, however, that several biological systems are also affected, including the central nervous system (CNS). Neurological manifestations such as stroke, encephalitis, and psychiatric conditions have been reported in COVID-19 patients, but the neurotropic potential of the virus is still debated. Herein, we sought to investigate SARS-CoV-2 infection in human neural cells. We demonstrated that SARS-CoV-2 infection of neural tissue is non-permissive, however it can elicit inflammatory response and cell damage. These findings are consistent with the hypothesis that most of the neural damage caused by SARS-CoV-2 infection is due to a systemic inflammation leading to indirect harmful effects on the CNS despite the absence of local viral replication.

Author Summary

Severe acute respiratory syndrome coronavirus 2 (SARS-CoV-2) is the causative agent of Coronavirus disease 2019 (COVID-19). COVID-19 was initially described as a pulmonary disease, however, with an increased number of patients showing neurological manifestations, the SARS-CoV-2 neurotropism became an important issue. It is still unclear whether the new coronavirus causes direct damage to the neural tissue or if the neurological symptoms are the result of systemic vascular and inflammatory responses. Here, we investigated the consequences of the infection of human neurospheres by SARS-CoV-2. Despite SARS-CoV-2 RNA occurrence in the supernatant of neurospheres, we did not detect viral particles with infective capacity. Nevertheless, we observed some neuroinflammatory markers and cell cytotoxicity as a consequence of viral infection. Our study suggests that the impact of virus infection in the CNS is limited and massive damage may be caused by general inflammation.

Introduction

Severe acute respiratory syndrome coronavirus 2 (SARS-CoV-2) is the causative agent of the 2019 coronavirus disease (COVID-19), an airborne infectious disease. Most affected patients have symptoms of respiratory infections, such as fever, dry cough and dyspnea, and 5 to 10% of them evolve to severity/death. Respiratory failure is the main event that explains fatality in COVID-19. Some authors raised the possibility that at least part of the respiratory manifestations caused by COVID-19 could be due to direct viral damage to the respiratory center located in the brain stem [1].

Apart from respiratory symptoms, anosmia and ageusia were identified as hallmarks of COVID-19. Indeed, evidence of neurological disease associated with COVID-19 is increasing; 30 to 60% of patients further present one or more neurological symptoms, including paresthesia, altered consciousness, and headache [2,3]. Besides, COVID-19 patients are at a 7-fold higher risk to suffer a stroke, and 2-6% progress to cerebrovascular disease [4]. Less frequent neurological manifestations include encephalopathy, encephalitis and Guillain-Barré syndrome [5,6].

Neuroinvasive capacity was shown for other highly pathogenic coronaviruses, including the Middle East Respiratory Syndrome coronavirus (MERS-CoV) [7] and SARS-CoV [8,9]. Similarly to SARS-CoV, SARS-CoV-2 uses the angiotensin-converting enzyme 2 (ACE2) receptor as the main cellular entry [10]. ACE2 is highly expressed in nasal epithelial cells, which underlies the initiation of respiratory tract infection [11], but is also present in multiple tissues [12].

Studies dissecting the putative mechanisms whereby SARS-CoV-2 enters the central nervous system (CNS) are still scarce. At first, it was speculated that the virus infects the olfactory neurons and reaches the brain by anterograde axonal transport. However, it was shown in rodents that SARS-CoV-2 infects non-neural cells in the olfactory epithelium rather than olfactory neurons, which could be attributed to the lack of expression of ACE2 in these cells [13,14]. In contrast, a recent *postmortem* study found viral particles throughout olfactory neuron projections and in the olfactory bulb of a few patients [15]. Therefore, due to these conflicting findings, it is still debatable whether the mechanism of SARS-CoV-2 invasion in the CNS is via olfactory neurons.

Viral infections targeting the brain were successfully modeled *in vitro* using human neurospheres (NP) and brain organoids [16,17], so these models have been chosen to investigate whether SARS-CoV-2 infects the brain tissue. While some researchers found that the virus infects neurons and glia [18–20], others were unable to

detect viral antigens in these cells [21], suggesting SARS-CoV-2 neural infection was dependent on experimental conditions and/or viral isolates.

Here, we investigated SARS-CoV-2 infection in NP. Although viral infection was found to be non-permissive, it led to inflammatory response and cytotoxicity which was correlated to the amount of virus in the inoculum. Therefore, we suggest that despite insufficient viral infection and replication in the brain parenchyma, there are consequences of the viral presence in the tissue, which may be enhanced by the entry of inflammatory molecules resulting from a generalized inflammatory response.

Results

SARS-CoV-2 replication in neural cells is non-permissive

Histopathological analyses of several tissues from an infant deceased with COVID-19 fully described in a case report from our group [22], showed viral presence by immunofluorescence (IF) with anti-SARS-CoV-2 spike protein (SP) in the ChP, LV lining, and in some locations of the frontal cerebral cortex (S1A Fig). SARS-CoV-2 infection was confirmed by quantitative Reverse Transcriptase–Polymerase Chain Reaction (qRT-PCR) (S1B Fig). The heart and the lungs, which have been previously demonstrated to be permissive to SARS-CoV-2 infection [23–26], also showed presence of the virus (S1 Fig and [22]). We sought to verify whether the expression levels of ACE2 receptor could explain the differences in viral infection in different brain areas, compared with the expression in the heart and lungs, which are known to be infected by SARS-CoV-2. Data from Protein Atlas and Allen Brain Atlas databases were used for comparison [27,28]. We found that ChP had higher ACE2 levels than other brain regions assessed (Fig 1A) and the heart and lungs expressed higher levels of ACE2 in comparison with most neural tissues (Fig 1A).

NP cultivated *in vitro* reproduced the low expression of ACE2 mRNA of brain parenchyma, so we decided to compare it to human iPS-derived cardiomyocytes (CM), a cell type know to express higher amount of ACE2 receptor and also used as an *in vitro* model for cardiac infection [24,29]. NP show lower ACE2 expression (Fig 1B), validating their use as a neural model of SARS-CoV-2 infection *in vitro*.

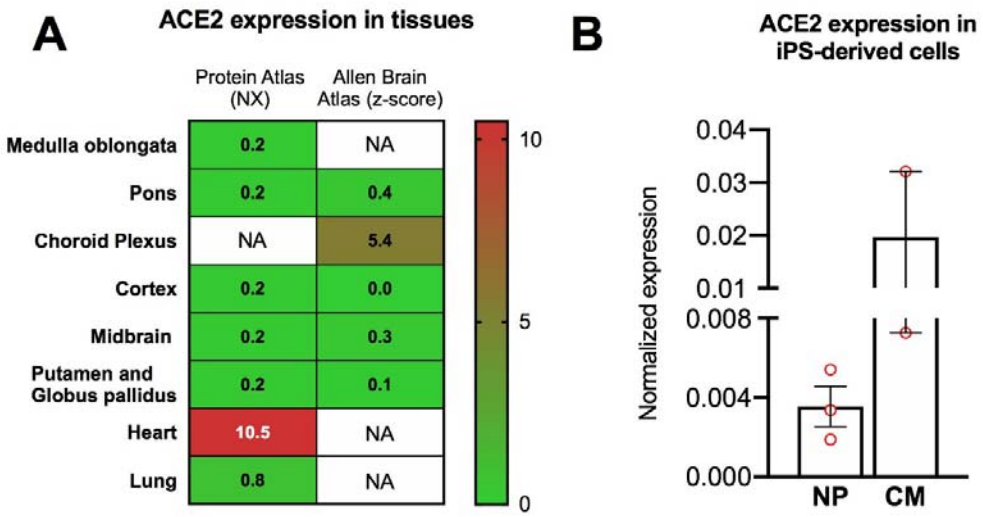

Fig 1. ACE2 expression in human tissues and iPSC-derived cells. (A) ACE2 expression in human tissues based on Protein Atlas and Allen Brain Atlas databases. Consensus normalized expression (NX) and z-score are used to represent the relative abundances within the respective databases (Citations in the main text). NA= not analyzed (B) Relative mRNA expression levels of ACE2 in iPSC-derived cultures: NP and CM (n=3 for NP and n=2 for CM), normalized to reference genes.

SARS-CoV-2-infection in NP was addressed using multiplicity of infection (MOI) (0.01 and 0.1) and time of exposure to the viral particles (1h) known to infect other virus permissive cells, such as CM, Vero and Calu-3 cells [24,29–31]. Five days post infection (d.p.i.), SARS-CoV-2 could not be detected by immunostaining for double-stranded (ds)RNA (Fig 2A). Additionally, infected NP did not stain for SARS-CoV-2 convalescent sera (CS) (S2A Fig). In contrast, NP infected with Zika virus (ZIKV) were immunoreactive for dsRNA (arrows, Fig 2A), and CM infected with SARS-CoV-2 were immunoreactive for dsRNA and CS (arrows, Fig 2A and S2B Fig, correspondingly). Western blotting (WB) of NP at 2 d.p.i. also showed the absence of viral proteins, using both anti-SARS-CoV-2 SP (Fig 2B) and anti-SARS-CoV-2 CS (S2C Fig). On the other hand, infected Vero cells showed prominent bands corresponding to the molecular weights of SARS-CoV-2 spike protein and nucleoprotein, as detected by anti-SARS-CoV-2 SP (Fig 2B) and anti-SARS-CoV-2 CS (S2C Fig), respectively.

Despite the absence of SARS-CoV-2 detection, the supernatant of NP harvested 5 d.p.i. showed approximately 10^4 and 10^5 copies of genomic and subgenomic viral RNA, respectively, which were at least 4 orders of magnitude lower than the

observed in infected Vero cells (Fig 2C). The infectivity of the viral particles in the supernatant of NP (MOI 0.1), addressed by plaque forming unit (PFU) assay, showed no infective viral progenies at 2 and 5 d.p.i, whereas for CM at 2 d.p.i. there was on average 2.8 x 10^6 PFU/mL (data not shown) (Fig 2D). The analysis of the virus inoculum in NP at day 0 contained on average 3 x 10^3 PFU/mL, confirming that they were exposed to infectious virus particles (Fig 2D). The aforementioned detection of RNA virus contrasts with the absence of infectious virus progeny and may indicate that neural cells were a dead-end for SARS-CoV-2 infection, or that the viral RNA detected in the supernatant was a residual of the inoculum.

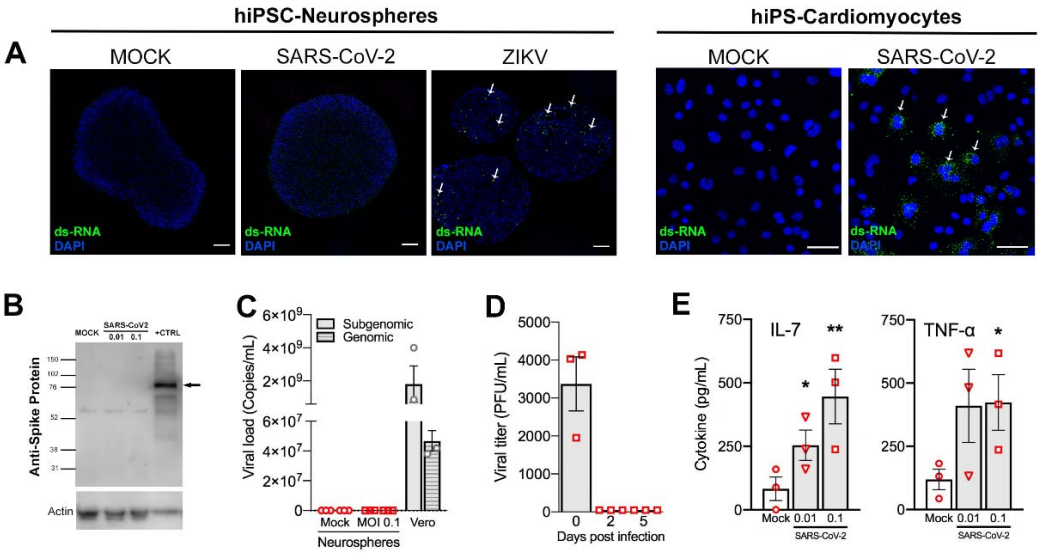

Fig 2. SARS-CoV-2 replication in NP is non-productive. (A) IF staining for SARS-CoV-2, with anti-dsRNA (green), in cryosections of 5 d.p.i. NP (MOI 0.1). Nuclei were counterstained with DAPI (blue). ZIKV-infected NP (MOI 0.5 for 72h) and SARS-CoV-2-infected CM (MOI 0.1 for 48h) were used as positive controls for dsRNA labeling and SARS-CoV-2 infectivity, respectively. Scale bar: 50 µm (B) Detection of SARS-CoV-2 SP by WB. Protein extracts from Vero cells (MOI 0.1 for 24h) were used as positive control. Gel loading was assessed by beta-actin staining. (C) Real-time qRT-PCR of genomic and subgenomic RNA levels of SARS-CoV-2 in the supernatants of NP 5 d.p.i. SARS-CoV-2-infected Vero cells were used for comparison. (D) Plaque forming units assay from the supernatants of the NP at 2 and 5 d.p.i (MOI 0.1). Data was plotted as average plus standard error. (E) Multiplex luminex assay for IL-7 and TNF-α from the supernatant of NP

collected 5 d.p.i. (*p<0.05, **p<0.005). Collected data corresponds to the infection of NP from 3 different cell lines in one experimental infection.

SARS-CoV-2 infection of neural cells triggers an increase in pro-inflammatory cytokines

SARS-CoV-2 infection has been associated with cytokine storm as a poor prognosis of disease progression [32]. Misbalance of cytokine levels in the CNS microenvironment is associated with several pathologies [33–36], hence the need to uncover the brain inflammation associated with SARS-CoV-2 infection. To investigate if SARS-CoV-2 generates a direct inflammatory response in neural tissues, the supernatant of infected NP was collected at 5 d.p.i. and analyzed by Multiplex Luminex assay to measure over 20 cytokines and chemokines (Fig 2E and S3 Fig). The levels of IL-7 and TNF-α in the infected NP were higher compared with mock condition (Fig 2E). The levels of other cytokines and chemokines were not affected by SARS-CoV-2 infection in these conditions (S3 Fig).

Prolonged exposure to higher inocula of SARS-CoV-2 does not elicit permissive infection of NP.

The exposure time of NP to the virus inoculum and the low MOIs are sufficient to detect the virus in permissive cells, including Vero and CM. The same conditions, in contrast, did not prompt the detection of viral particles by neither IF nor WB in NP nor even infective particles in the culture supernatant. Arguably, this evidence of non-permissiveness could be explained by insufficient exposure time of the cells during viral inoculation. A previous report showed infection of NP after 24 h inoculation time at higher MOIs [37]. Additionally, it is speculated that the initial amount of virus in the inoculum is crucial in determining the severity of COVID-19 symptoms [38]. To clarify these questions and to better compare our results with data published by others, NP were then exposed to a longer infection time and to higher MOIs.

We compared the capacity of SARS-CoV-2 to generate infectious viral particles in NP using 1h and 24h incubation times and MOIs of 0.1, 1 and 10. Despite longer exposure and higher viral titer, these conditions also did not support the production of novel infective particles, as measured by plaque forming units assay of the respective supernatants (Fig 3A). However, SARS-CoV-2 SP was detectable by IF in NP incubated for 24h with the virus and analyzed 24h post infection (Fig 3B). On the other hand, after

48h and 72h of the same 24h-infection, the NP had no detectable SP immunostaining, suggesting that viral proteins are only present transiently (Fig 3B and S2D Fig). Remarkably, at a time point in which no virus could be detected in NP, LDH measurements of culture supernatants revealed increased cytotoxicity at MOI 1 and 10, irrespective of incubation time with the virus inoculum (Fig 3C). These data indicate that exposure of NP to SARS-CoV-2 at high MOIs is neurotoxic and that, likely, death of infected cells is responsible for the decline of virus titers over time (Fig 3). Also, the incubation time with the inoculum does not seem to affect the outcome of infection, since prolonged exposure time did not increase the production of viral particles or augment the extent of cell damage.

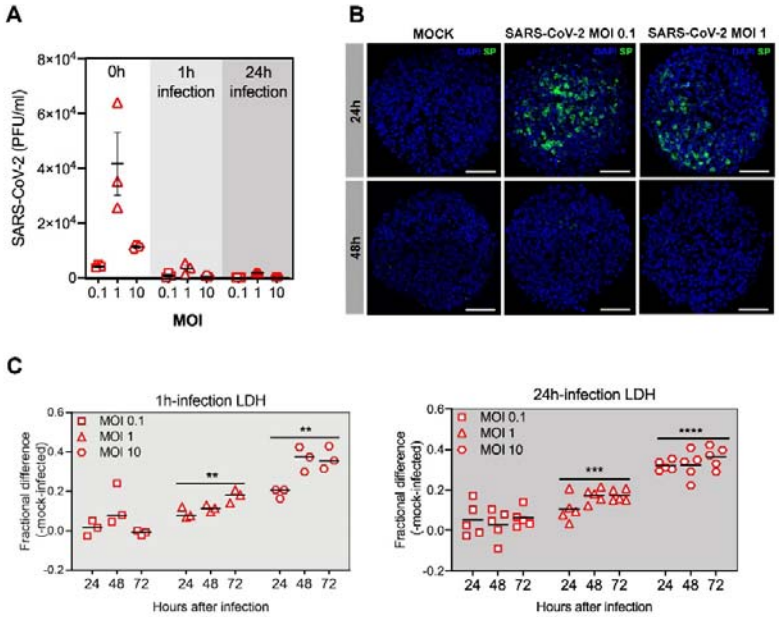

Fig 3. Prolonged exposure to higher inocula of SARS-CoV-2 does not elicit permissive infection of NP but higher MOIs are cytotoxic. NP were inoculated with SARS-CoV-2 for 1 h or 24 h at indicated MOIs. (A) After 72h post-infection, culture supernatants were harvested to quantify infectious virus titers in Vero Cells by plaque forming units assay. (B) NP inoculated for 24 h were immunostained with anti-SARS-CoV-2 SP (green) and counterstained with DAPI (blue) at 24h and 48h post-infection. Scale bars: 40 µm (C) Lactate Dehydrogenase (LDH) levels were measured by colorimetric assay in NP inoculated for 1h and 24h at 24h, 48h and 72h post infection. Data points correspond to measurements from single NP from one experimental infection.

Strain differences in SARS-CoV-2 RNA sequence could explain distinct infectivity of neural cells

Genetic variation in SARS-CoV-2 isolates has been described and could help to explain differences in the infectivity of neural tissue previously reported [39]. To investigate whether possible genetic components could account for the differences between SARS-CoV-2 infections reported in literature and in the current work, we compared the phylogeny of the nucleotide sequences of our strain with the strains used in these works, by means of the Wuhan strain genome as reference. The analysis showed less than 1% variation among the genetic sequences of our strain, Zhang and collaborators, and Song and collaborators (Table 1) [20,37]. These small variations correlate with mutations in the receptor-binding domain of Spike protein and two non-structural proteins (nsp) (Table 2).

Table 1. Estimates of evolutionary divergence between SARS-CoV-2 sequences.

Virus Strain	NC_045512.2 Wuhan-01	MT710714.1 This study	MT230904.1 Zhang et al	MT020880.1 Song et al	MT246667.1 Song et al
MT710714.1 - This study	0.06	-	-	-	-
MT230904.1 - Zhang et al	0.03	0.09	-	-	-
MT020880.1 - Song et al	0.01	0.07	0.04	-	-
MT246667.1 - Song et al	0.01	0.07	0.04	0.00	
MN985325.1 - Song et al	0.01	0.07	0.04	0.00	0.00

The values correspond to the divergence in sequences of SARS-CoV-2 when comparing the strain in rows with the strain in columns. Sequences were compared with maximum likelihood phylogenetic analysis as described in the Material and Methods section.

Table 2. Specific proteins mutations between SARS-CoV-2 strains.

Virus Strain	NSP2	NSP7	NSP14	SPIKE (RBD)	SPIKE	M	ORF8
MT710714.1 - This study	T265I	S3884L			D614G		
MT230904.1 - Zhang et al				V367F		C207R	R183P
MT020880.1 - Song et al			S5932F				
MT246667.1 - Song et al			S5932F				
MN985325.1 - Song et al			S5932F				

Each amino acid mutation was accessed through sequence pairing comparison to the SARS-CoV-2 reference genome (Wuhan-Hu-1).

Our viral isolate presented three missense mutations compared to the Wuhan sequence: D614G on spike protein, S3884L on nsp7 and T265I on nsp2. The D614G spike protein mutation has been correlated with more infectious behavior of the strain [39]. Nsp 7 participates in SARS-CoV-2 replication, being a co-factor for RNA polymerase. The nsp2 role is unknown and may be related to the disruption of intracellular host signaling and mitochondrial biogenesis [40].

Discussion

Neurological manifestations of COVID-19 fueled research on the putative viral infection of the brain. However, absence or low detection of SARS-CoV-2 was described in the cerebrospinal fluid (CSF), and so far many reports have described the presence of SARS-CoV-2 in the brain parenchyma [20,26,41,42]. Here, we bring the attention to SARS-CoV-2 infection in the ChP in its LV lining, and in the frontal cortex of an infant's brain (S1A Fig), which was confirmed by qRT-PCR for viral RNA (S1B Fig) (pathological analysis of this case was described in detail in [22]).

The detection of SARS-CoV-2 was more pronounced in the ChP than in the cortex (S1A Fig). This matches expression data for the SARS-CoV receptor ACE2, which is enriched in ChP both *in vivo* and *in vitro*, in comparison to other brain areas, including cortex [18,21] (Fig 1A). Our protocol for differentiating NP generates cortical brain-like

tissue [43], which recapitulates the low expression levels of ACE2 mRNA observed in the human cortical tissue (Fig 1B). ACE2 levels are increased in patients with comorbidities, suggesting a relationship between ACE2 expression and susceptibility to severe COVID-19 [44]. Strategies to regulate the expression of ACE2 have been proposed as therapies to fight viral infection [45,46]. Also, it remains unaddressed if neuropsychiatric conditions and neurodegenerative diseases impact the expression of ACE2 in the brain [47] and how they could interfere with the susceptibility of CNS infection. Indeed, there is an increased risk for mental illness in COVID-19 patients, especially those who had previously psychiatric episodes [48]. In this context, human NP and brain organoids could be a model for *in vitro* drug testing, including monitoring changes in ACE2 expression and correlation with susceptibility to SARS-CoV-2 infection.

One experimental aspect that drew our attention was the amount of virus used to infect cells in other studies. Previous reports have demonstrated SARS-CoV-2 antigens in NP and brain organoids [19,20,37] using MOIs at least 100 times higher than the lowest MOI used in our investigation. Although productive infection in neural cells was claimed at MOI 10 [37], we did not obtain infectious viral particles at similar experimental conditions (Fig 2D).

The genetic comparison between our strain and the strains of other works showed little variations (Table 1) that, nevertheless, caused potentially significant alterations in the amino acid sequence of viral proteins (Table 2). Indeed, most of these variations might reflect the genetic diversity of the SARS-CoV-2 since the original outbreak [49]. The strain used in the current work has a D614G mutation that renders the virus highly infectious by increasing ACE2 interaction [39]. This D614G spike mutation has also been associated with increased binding of neutralizing antibodies [50]. Our strain has also a mutation in a cofactor of SARS-CoV-2 RNA-dependent RNA polymerase, nsp7, that did not lead to impairments in viral replication in permissive cells such as Vero (Fig 2C), however, this mutation could not be excluded as responsible for the differences observed between the studies. Finally, the T265I nsp2 mutation falls within the extracellular N-terminus of the protein [51] and is thought to cause structural changes, and which can now be found in all geographical locations [52]. Similarly to our work, Zhang and collaborators have also used a strain with increased sensitivity to neutralizing antibodies [53]. On the other hand, Song and collaborators used a viral strain that is not world spread [54–56] and it has been reduced in frequency over time since February 2020 [56]. In addition, the S5932F mutation on nsp14 (ExoN), could lead to altered proofreading exonuclease activity via weaker interaction with nsp10, facilitating the emergence of diverse viral sequences with potential selective advantage [57].

Cells from lungs, intestine, heart and kidney, which have already been demonstrated to be sites of infection [25,58–60], produce infectious viral progeny *in vitro* with MOIs ranging from 0.01 to 1 [30,31]. Therefore, it seems unlikely that even in severe neuro-COVID cases such as the one cited here, neural cells would be exposed to quantities equal to or more than one plaque forming virus per cell. Our observation that ChP is infected to a much greater extent than other regions of the brain, together with the lack of infectious virus particles *in vitro* with MOI < 1, argue against the clinical relevance of using high titers of SARS-CoV-2 for modeling the infection *in vitro*. A study using viral titers of MOI 0.5 showed that SARS-CoV-2 exclusively infects ChP cells in brain organoids, but no other cell types. In the same report, even at higher viral titers (MOI 10), infection of neurons was minor [21]. Our observation that SARS-CoV-2 infects the ChP without significantly spreading to other brain areas (S1 Fig) and the absence of a productive infection in human NP with SARS-CoV-2 at MOI of 0.1, 1 and 10 even at increased inoculation time (Fig 3), corroborate these findings.

Despite non-permissiveness to SARS-CoV-2 infection of the brain parenchyma, the data presented here also points to direct pro-inflammatory and cytotoxic response of this tissue. This direct effect is probably related to the number of viral particles able to first get in contact with the CNS. It was observed in NP an increase in IL-7 and TNFα levels following infection with low MOIs, but not of other inflammatory cytokines such as IL-6. IL-7 has antiviral activity [61] and neurotrophic effects in neurons [62,63] and its increase at MOIs 0.01 and 0.1 may correlate with a protective neuroimmune response dependent on virus titer amount. TNF-α is secreted by astrocytes and microglia in response to injury, including viral infection, inducing neuronal damage [64]. It also regulates the permeability of the blood-brain barrier and neuronal plasticity [65,66]. Certainly, these results are interesting with respect to a direct inflammatory response from neural cells that had been in contact with SARS-CoV-2 and deserve further experiments. It is expected that in the complex scenario of the response to viral infection, multiple cytokines are regulated promoting cell protection and also limiting infection by inducing cell death. Therefore, the extent of neural damage should correspond to a balance between these responses.

This work supports the hypothesis that the infection of ChP with SARS-CoV-2 may change CNS homeostasis to increase the permeability of the blood-CSF barrier. Virus particles reaching the brain parenchyma can trigger inflammatory response leading to tissue damage. Notably, neurological symptoms are more frequent in severe patients with exacerbated inflammation, compared to mild or moderate ones, suggesting that an overall increase in the inflammatory response may set place for CNS damage [6]. Low type I interferon response in infants' brains may correlate with higher susceptibility for

virus entry in CNS, but also patients with previous neurological and psychiatric disorders which may have weakened immune response or enhanced inflammation should be closely monitored [48,67].

Materials and methods

Cell cultivation

Human induced pluripotent stem (iPS) cells were obtained from the Coriell Institute for Medical Research repository (GM23279A) or produced in house with CytoTune™-iPS 2.0 Sendai Reprogramming Kit (A16517- Invitrogen) from skin fibroblasts [68] or urine epithelial cells [69]. iPS cells were cultured in StemFlex media (A33494 - Thermo Fisher Scientific01) on top of Matrigel (BD Biosciences, Franklin Lakes, NJ). NSCs are generated from human-induced pluripotent stem cells (hiPSCs) following the published Life Technologies protocol for Induction of Neural Stem Cells from Human Pluripotent Stem Cells (Publication number: MAN0008031). NSCs were grown in neural expansion medium (Advanced DMEM / F12 and Neurobasal medium (1: 1) with 1% neural induction supplement) on a surface previously coated with Geltrex LDEV-Free (Thermo Fisher Scientific, A1413302) and when cells reached 90% confluence the culture was split with Accutase (Merck Millipore, SCR005).

NP were prepared in suspension as follows: upon reaching 90% of confluence, 3 x 10^6 NSCs were split and plated in a 6 well-plate well and cultured on an orbital shaker at 90 rpm for 7 days in standard culture conditions. The culture medium was composed of Neurobasal medium/DMEM-F12 1:1, supplemented with 1x N2 (Thermo Fisher Scientific) and 1x B27 (Thermo Fisher Scientific), and it was changed each 3-4 days [70]. Alternatively, NP were prepared directly in 96 well plates. After NSCs reached 90% of confluence, cells were split with Accutase (Merck Millipore, SCR005) and counted on the Neubauer chamber. Cells were then centrifuged at 300 x*g* for 5 minutes and resuspended in neural medium with half DMEM / F12 (Life Technologies, 11330-032) and half Neurobasal medium (Thermo Fisher Scientific, 12348017) supplemented with 1x N2 (Invitrogen 17502001) and 1x B27 (Thermo Fisher Scientific, 17504001) supplements. Subsequently, 9 x 10^3 cells in 150 μL were plated per well of a round bottom Ultra-low attachment 96 well plate (Corning, 7007), followed by centrifugation at 300 x*g* for 3 minutes to assure sedimentation. To minimize neurosphere damage, the medium of each well was changed every other day by only removing 70-100 μL and adding 150 μL of new medium. iPSC derived human cardiomyocytes were purchased from Pluricell (São Paulo,

Brazil) [71]. CMs were used between day 25 and day 35 of differentiation, and average cell purity by cardiac specific troponin T protein was 86%.

Total RNA isolation

Seven days-old NP were cultured in 6-well plates, harvested and immediately frozen at -80°C until further processing. Total RNA isolation was performed using ReliaPrep™ RNA Tissue Miniprep System (Promega Corporation) according to manufacturer's instructions. For cardiomyocytes, total RNA was isolated using TRIzol™ reagent, according to manufacturer's recommendations (Thermo Fisher Scientific). RNA concentration and quality were quantified on a NanoDrop™ 2000c Spectrophotometer (Thermo Fisher Scientific); and integrity and purity were evaluated by 1.8% agarose gel electrophoresis using a photo documentation device equipped with a UV lamp (L-PIX, Loccus Biotecnologia). Then, samples were digested with DNase I, Amplification Grade, following the manufacturer's instructions (Invitrogen, Thermo Fisher Scientific). 2 µg of RNA from DNAse-treated samples were reverse transcribed using M-MLV for complementary DNA generation (cDNA) (Thermo Fisher Scientific).

Quantitative Reverse Transcriptase–Polymerase Chain Reaction (qRT-PCR)

For gene expression analysis of NP and cardiomyocytes, qRT-PCR reactions were conducted in three replicates with a final reaction volume of 10 µL in MicroAmp Fast Optical 96 Well Reaction Plates (Thermo Fisher Scientific) containing 1X GoTaq qPCR Master Mix (Promega Corporation), 300 nM CXR Reference Dye, a final concentration of 200 nM of each SYBR green designed primers [Angiotensin I Converting Enzyme 2 (ACE2; forward: 5'-CGAAGCCGAAGACCTGTTCTA-3'; reverse: 5'-GGGCAAGTGTGGACTGTTCC-3') ThermoFisher Scientific] and 10 ng of cDNA per reaction. Appropriate controls (no reverse transcriptase and template-negative controls) were incorporated into each run. Briefly, the reactions were performed on a StepOnePlus™ Real-Time PCR System thermocycler (Applied Biosystems). Thermal cycling program comprised of a denaturing step at 95°C for 3 min, followed by 40 cycling stages at 95°C for 15 sec, 57°C for 15 sec, 72°C for 15 sec and melt curve stage 95 °C, 15 sec; 60 °C, 1 min; 95 °C, 15 sec. The relative expression of the genes of interest was normalized by human reference genes: Glyceraldehyde-3-phosphate Dehydrogenase (GAPDH; forward: 5'-GCCCTCAACGACCACTTTG-3'; reverse: 5'-CCACCACCCTGTTGCTGTAG-3') and Hypoxanthine Phosphoribosyltransferase 1 (HPRT-1; forward 5'-CGTCGTGATTAGTGATGATGAACC-3'; reverse: 5'-AGAGGGCTACAATGTGATGGC-3'). qPCR data analysis was performed with the N_0

method implemented in LinRegPCR v. 2020.0, which considers qPCR mean efficiencies estimated by the window-of-linearity method [72,73]. Briefly, N_0 values were calculated in LinRegPCR using default parameters. Then, the arithmetic mean of N_0 values from gene of interest (GOI) was normalized by taking its ratio to the N_0 geometric mean of the reference genes (REF: *GAPDH and HRRT-1*; N_{0GOI}/N_{0REF}).

SARS-CoV-2 propagation

SARS-CoV-2 obtained from a nasopharyngeal swab from a confirmed case in Rio de Janeiro, Brazil (GenBank accession no. MT710714) was expanded in African green monkey kidney cells (Vero, subtype E6). Virus isolation was performed after a single passage in cell culture in a 150 cm^2 flask, previously infected with SARS-CoV-2 at multiplicity of infection (MOI) 0.01. All procedures related to virus culture were handled in a biosafety level 3 (BSL3) facility, according to WHO guidelines. Virus stocks were kept at -80°C.

Cell infection

Seven days-old NP were infected with SARS-CoV-2 at MOI 0.1 (9×10^2 PFU per neurosphere). Following 1h incubation, the inoculum was partially replaced by fresh medium and NP were cultured for additional 2 and 5 days, with orbital shaking at 90 rpm in standard conditions (5% CO_2 and 37°C). The medium was not completely replaced to avoid excessive stress as explained above. NP exposed to uninfected Vero's culture medium were used as controls of infection (Mock). NP (≈ 50 to 200) were used per experimental group for each analysis. Culture supernatants were collected at 2 and 5 days post-infection for virus titration by plaque forming units (PFU) assay and/or real time qRT-PCR. The assay was performed in a single experiment, consisting of three cell lines generated from 3 independent donors.

In lieu of the formerly described method, seven days-old NP were separately (one per well) infected for 1h or 24h with SARS-CoV-2 at different MOIs (0.1, 1 and 10; 9×10^3 cells per neurosphere). After incubation, the inoculum was partially replaced by fresh medium, for the reasons stated above, and NP were cultured in standard conditions (5% CO_2 and 37°C). Supernatants and NP were collected at 24h, 48h and 72h post-infection. NP exposed to uninfected Vero's culture medium were used as controls of infection (Mock). 5 to 24 NP were distributed by each experimental group.

Cardiomyocytes were infected with SARS-CoV-2 at MOI 0.1 for 1h. Next, the inoculum was replaced by fresh medium and cultured in standard conditions for 48-72 h.

After that, the monolayer was fixed with 4% paraformaldehyde (PFA) solution and the supernatant was harvested for cytokine evaluation.

Immunofluorescence staining

NP were fixed in 4% paraformaldehyde solution (Sigma-Aldrich) for 1h, followed by cryopreservation with 30% sucrose solution overnight. Then, samples were embedded in O.C.T compound (Sakura Finetek, Netherland) and frozen at -80˚C. The O.C.T blocks were sectioned at 20 µm-slices with a Leica CM1860 cryostat. After washing with PBS, sections were incubated in permeabilization/blocking solution (0.3% Triton X-100/ 3% goat serum) for 2h. The primary antibody was incubated overnight at 4˚C [anti-double-stranded RNA (dsRNA) monoclonal antibody (1:200, Scicons)]. Then, sections were incubated with secondary antibody goat anti-mouse Alexa Fluor 488; 1:400, A-11001 - Thermo Fisher Scientific) for 2h. Nuclei were counterstained with 0.5 µg/mL 40-6-diamino-2-phenylindole (DAPI) for 10 minutes and the slides were mounted with Aqua-Poly/Mount (Polysciences).

After fixation, cardiomyocytes were washed with PBS and then incubated with permeabilization/blocking solution (0.3% Triton X-100 / 3% bovine serum albumin) for 1h. Then, cells were incubated with primary antibody anti-dsRNA (1:200) overnight at 4ºC. Day after, cells were incubated with the secondary antibody goat anti-mouse Alexa Fluor 488 (1:400) for 1h. Nuclei were counterstained with DAPI for 5 minutes and mounted with 50% PBS-Glycerol.

Images of NP and cardiomyocytes were acquired on a Leica TCS-SP8 confocal microscope with the 63x and 20x objective, respectively.

Plaque forming unit assay

For virus titration, monolayers of Vero E6 cells (2 x 10^4 cell/well) in 96-well plates were infected with serial dilutions of supernatants containing SARS-CoV-2 for 1 hour at 37°C. Semi-solid high glucose DMEM medium containing 2% FSB and 2.4% carboxymethylcellulose was added and cultures were incubated for 3 days at 37 °C. Then, the cells were fixed with 10% formalin for 2 h at room temperature. The cell monolayer was stained with 0.04% solution of crystal violet in 20% ethanol for 1 h. Plaque numbers were scored in at least 3 replicates per dilution by independent readers blinded to the experimental group and the virus titers were determined by plaque-forming units (PFU) per milliliter.

Molecular detection of SARS-CoV-2 RNA

The total RNA from neurosphere's supernatant was extracted using QIAamp Viral RNA (Qiagen), according to manufacturer's instructions. Quantitative RT-PCR was performed using QuantiTect Probe RT-PCR Kit (Quiagen®) in a StepOne™ Real-Time PCR System (Thermo Fisher Scientific). Amplifications were carried out in 25 µL reaction mixtures containing 2X reaction mix buffer, 50 µM of each primer, 10 µM of probe, and 5 µL of RNA template. Primers, probes, and cycling conditions recommended by the Centers for Disease Control and Prevention (CDC) protocol were used to detect the SARS-CoV-2 (https://www.fda.gov). Alternatively, genomic (ORF1) and subgenomic (ORFE) were detected, as previously described [74].

Western blot analysis

After 2 days post-infection (d.p.i), 100 µL of sample buffer without bromophenol blue (62.5 mM Tris-HCl, pH 6.8, containing 10% glycerol, 2% SDS and 5% 2-mercaptoethanol) was added to the NP and, then, samples were frozen at -80°C. Next, samples were gently broken down with a disposable pestle (BAF 199230001- Sigma, Bel-Art) and cell extracts were boiled at 95°C for 10 min and centrifuged at 4°C 16,000x g for 15 min to remove insoluble material. Protein content was estimated using the Bio-Rad Protein Assay (#5000006, Biorad). After addition of bromophenol blue (0.02%), extract samples (40 µg/lane for NP and 15 µg/lane for Vero cells) were separated by electrophoresis on a 10% SDS polyacrylamide gel and transferred to polyvinylidene difluoride (PVDF) membranes. Membranes were blocked in 5% non-fat milk in Tris-Buffered Saline with 0.1% Tween-20 (TBS-T) for 1 hour at room temperature. Membranes were then incubated overnight at 4°C, in the presence of anti-SARS-CoV-2 SP (1:2,000, #GTX632604 - GeneTex) and anti-actin (1:2000, MAB1501, Millipore) diluted in TBS-T with 5% non-fat milk. Then, membranes were incubated with peroxidase-conjugated antibody goat anti-Mouse IgG (H+L), HRP-conjugate (1:10,000, G21040 -Molecular Probes). The signals were developed using ECL Prime Western Blotting System (#GERPN2232, Sigma) for five minutes and chemiluminescence was detected with an Odyssey-FC System® (Imaging System - LI-COR Biosciences). Membranes were also stripped for re-staining by incubating for three cycles of 10 minutes in stripping buffer (pH 2.2, 200 mM glycine, SDS 0,1% and 1% Tween-20), the buffer was discarded, then the membranes were washed for 5 minutes with PBS (three times) and 5 minutes with 0.1% TBS-T (three times). Next, the membranes were blocked again and processed for immunolabeling as described above.

Cytokine multiplex assay and LDH cytotoxicity assay

A multiplex biometric immunoassay containing fluorescent dyed microbeads was used to measure cytokines in the cell culture supernatant (Bio-Rad Laboratories, Hercules, CA, USA). The following cytokines were quantified: IL-1β, IL-1RA, IL-2, IL-4, IL-5, IL-6, IL-7, IL-8, IL-9, IL-10, IL-12(p70), IL-13, IL-15, IL-17, basic FGF, Eotaxin, G-CSF, GM-CSF, IP-10, MCP-1, MIP-1α, MIP-1β, PDGF-BB, RANTES, TNF-α, and VEGF; and cytokine levels were calculated by Luminex technology (Bio-Plex Workstation; Bio-Rad Laboratories, USA). The analysis of data was performed using software provided by the manufacturer (Bio-Rad Laboratories, USA). A range of 0.51–8,000 pg/mL recombinant cytokines was used to establish standard curves and the sensitivity of the assay. Cell death was determined according to the activity of lactate dehydrogenase (LDH) in the culture supernatants using a CytoTox® Kit (Promega, USA) according to the manufacturer's instructions.

Statistics were performed using GraphPad Prism software version 8. Numerical variables from NP experiments were tested regarding their distribution using the Shapiro-Wilk test. For those following a normal (parametric) distribution, One-way analysis of variance (ANOVA) with Dunnet's post-hoc test was used to compare differences among groups; and for nonparametric data, Kruskal-Wallis test with Dunn's post-hoc test was used to compare differences.

SARS-CoV-2 strains sequence analyses

Nucleotide sequences from our strain (GenBank accession No. MT710714), from strains used in others works [20,37], and from SARS-CoV-2 reference genome (Wuhan-Hu-1, GenBank accession No. NC_045512.2) were retrieved from NCBI database and from Multiple Sequence Alignment (MSA). Visualization of SARS-CoV-2 sequences was performed using ClustalW [75] implemented in MEGA X program- version 10.1.8 [76]. Maximum Likelihood phylogenetic analyses were conducted using the JTT matrix-based model [77] with confidence assessed by bootstrap with 1,000 replicates. For identification of amino acid mutations, the coding data was translated assuming a Standard genetic code and compared to the SARS-CoV-2 reference genome Wuhan-Hu-1.

Acknowledgments

The authors would like to thank Claudia Figueiredo and Claudio Ferrari for helpful discussions during the elaboration of this manuscript; and Fernando Colonna Rosman and Leila Maria Cardão Chimelli for their support in the tissue's analysis.

References

1. Gupta A, Madhavan MV, Sehgal K, Nair N, Mahajan S, Sehrawat TS, et al. Extrapulmonary manifestations of COVID-19. Nature Medicine. 2020 Jul;26(7):1017–32.

2. De Felice FG, Tovar-Moll F, Moll J, Munoz DP, Ferreira ST. Severe Acute Respiratory Syndrome Coronavirus 2 (SARS-CoV-2) and the Central Nervous System. Trends Neurosci. 2020 Jun;43(6):355–7.

3. Wang L, Shen Y, Li M, Chuang H, Ye Y, Zhao H, et al. Clinical manifestations and evidence of neurological involvement in 2019 novel coronavirus SARS-CoV-2: a systematic review and meta-analysis. J Neurol. 2020 Jun 11;1–13.

4. Fifi JT, Mocco J. COVID-19 related stroke in young individuals. The Lancet Neurology. 2020 Sep 1;19(9):713–5.

5. Ellul MA, Benjamin L, Singh B, Lant S, Michael BD, Easton A, et al. Neurological associations of COVID-19. The Lancet Neurology. 2020 Sep 1;19(9):767–83.

6. Mao L, Wang M, Chen S, He Q, Chang J, Hong C, et al. Neurological Manifestations of Hospitalized Patients with COVID-19 in Wuhan, China: a retrospective case series study. medRxiv. 2020 Feb 25;2020.02.22.20026500.

7. Li K, Wohlford-Lenane C, Perlman S, Zhao J, Jewell AK, Reznikov LR, et al. Middle East Respiratory Syndrome Coronavirus Causes Multiple Organ Damage and Lethal Disease in Mice Transgenic for Human Dipeptidyl Peptidase 4. J Infect Dis. 2016 Mar 1;213(5):712–22.

8. Glass WG, Subbarao K, Murphy B, Murphy PM. Mechanisms of host defense following severe acute respiratory syndrome-coronavirus (SARS-CoV) pulmonary infection of mice. J Immunol. 2004 Sep 15;173(6):4030–9.

9. Xu J, Zhong S, Liu J, Li L, Li Y, Wu X, et al. Detection of Severe Acute Respiratory Syndrome Coronavirus in the Brain: Potential Role of the Chemokine Mig in Pathogenesis. Clin Infect Dis. 2005 Oct 15;41(8):1089–96.

10. Yan R, Zhang Y, Li Y, Xia L, Guo Y, Zhou Q. Structural basis for the recognition of SARS-CoV-2 by full-length human ACE2. Science. 2020 Mar 27;367(6485):1444–8.

11. Sungnak W, Huang N, Bécavin C, Berg M, Queen R, Litvinukova M, et al. SARS-CoV-2 entry factors are highly expressed in nasal epithelial cells together with innate immune genes. Nature Medicine. 2020 May;26(5):681–7.

12. Hamming I, Timens W, Bulthuis M, Lely A, Navis G, van Goor H. Tissue distribution of ACE2 protein, the functional receptor for SARS coronavirus. A first step in understanding SARS pathogenesis. J Pathol. 2004 Jun;203(2):631–7.

13. Brann DH, Tsukahara T, Weinreb C, Lipovsek M, Berge KV den, Gong B, et al. Non-neuronal expression of SARS-CoV-2 entry genes in the olfactory system suggests mechanisms underlying COVID-19-associated anosmia. Science Advances. 2020 Jul 31;6(31):eabc5801.

14. Bryche B, Albin AS, Murri S, Lacôte S, Pulido C, Gouilh MA, et al. Massive transient damage of the olfactory epithelium associated with infection of sustentacular cells by SARS-CoV-2 in golden Syrian hamsters. bioRxiv. 2020 Jun 16;2020.06.16.151704.

15. Meinhardt J, Radke J, Dittmayer C, Franz J, Thomas C, Mothes R, et al. Olfactory transmucosal SARS-CoV-2 invasion as a port of central nervous

system entry in individuals with COVID-19. Nature Neuroscience. 2020 Nov 30;1–8.

16. Garcez PP, Loiola EC, Costa RM da, Higa LM, Trindade P, Delvecchio R, et al. Zika virus impairs growth in human neurospheres and brain organoids. Science. 2016 May 13;352(6287):816–8.

17. Qian X, Nguyen HN, Song MM, Hadiono C, Ogden SC, Hammack C, et al. Brain-Region-Specific Organoids Using Mini-bioreactors for Modeling ZIKV Exposure. Cell. 2016 May 19;165(5):1238–54.

18. Jacob F, Pather SR, Huang W-K, Wong SZH, Zhou H, Zhang F, et al. Human Pluripotent Stem Cell-Derived Neural Cells and Brain Organoids Reveal SARS-CoV-2 Neurotropism. bioRxiv. 2020 Jul 28;2020.07.28.225151.

19. Mesci P, Macia A, Saleh A, Martin-Sancho L, Yin X, Snethlage C, et al. Sofosbuvir protects human brain organoids against SARS-CoV-2. bioRxiv. 2020 May 31;2020.05.30.125856.

20. Song E, Zhang C, Israelow B, Lu P, Weizman O-E, Liu F, et al. Neuroinvasive potential of SARS-CoV-2 revealed in a human brain organoid model. bioRxiv. 2020 Jun 26;2020.06.25.169946.

21. Pellegrini L, Albecka A, Mallery DL, Kellner MJ, Paul D, Carter AP, et al. SARS-CoV-2 infects brain choroid plexus and disrupts the blood-CSF-barrier. bioRxiv. 2020 Aug 21;2020.08.20.259937.

22. Gomes IC, Karmirian K, Oliveira J, Pedrosa C, Rosman FC, Chimelli L, et al. SARS-CoV-2 Infection in the Central Nervous System of a 1-Year-Old Infant Submitted to Complete Autopsy. 2020 Sep 13 [cited 2020 Oct 3]; Available from: https://www.preprints.org/manuscript/202009.0297/v1

23. Gnecchi M, Moretti F, Bassi EM, Leonardi S, Totaro R, Perotti L, et al. Myocarditis in a 16-year-old boy positive for SARS-CoV-2. Lancet. 2020 27;395(10242):e116.

24. Pérez-Bermejo JA, Kang S, Rockwood SJ, Simoneau CR, Joy DA, Ramadoss GN, et al. SARS-CoV-2 infection of human iPSC-derived cardiac cells predicts novel cytopathic features in hearts of COVID-19 patients. bioRxiv. 2020 Aug 25;2020.08.25.265561.

25. Tabary M, Khanmohammadi S, Araghi F, Dadkhahfar S, Tavangar SM. Pathologic features of COVID-19: A concise review. Pathol Res Pract. 2020 Sep;216(9):153097.

26. Schaller T, Hirschbühl K, Burkhardt K, Braun G, Trepel M, Märkl B, et al. Postmortem Examination of Patients With COVID-19. JAMA. 2020 Jun 23;323(24):2518–20.

27. Hawrylycz MJ, Lein ES, Guillozet-Bongaarts AL, Shen EH, Ng L, Miller JA, et al. An anatomically comprehensive atlas of the adult human brain transcriptome. Nature. 2012 Sep;489(7416):391–9.

28. Uhlén M, Fagerberg L, Hallström BM, Lindskog C, Oksvold P, Mardinoglu A, et al. Tissue-based map of the human proteome. Science [Internet]. 2015 Jan 23 [cited 2020 Oct 6];347(6220). Available from: https://science.sciencemag.org/content/347/6220/1260419

29. Marchiano S, Hsiang T-Y, Higashi T, Khanna A, Reinecke H, Yang X, et al. SARS-CoV-2 infects human pluripotent stem cell-derived cardiomyocytes, impairing electrical and mechanical function. bioRxiv. 2020 Aug 30;2020.08.30.274464.

30. Han Y, Yang L, Duan X, Duan F, Nilsson-Payant BE, Yaron TM, et al. Identification of Candidate COVID-19 Therapeutics using hPSC-derived Lung Organoids. bioRxiv. 2020 May 5;2020.05.05.079095.

31. Lamers MM, Beumer J, Vaart J van der, Knoops K, Puschhof J, Breugem TI, et al. SARS-CoV-2 productively infects human gut enterocytes. Science. 2020 Jul 3;369(6499):50–4.

32. Tay MZ, Poh CM, Rénia L, MacAry PA, Ng LFP. The trinity of COVID-19: immunity, inflammation and intervention. Nature Reviews Immunology. 2020 Jun;20(6):363–74.

33. Sochocka M, Diniz BS, Leszek J. Inflammatory Response in the CNS: Friend or Foe? Mol Neurobiol. 2017;54(10):8071–89.

34. Lima MC, de Mendonça LR, Rezende AM, Carrera RM, Aníbal-Silva CE, Demers M, et al. The Transcriptional and Protein Profile From Human Infected Neuroprogenitor Cells Is Strongly Correlated to Zika Virus Microcephaly Cytokines Phenotype Evidencing a Persistent Inflammation in the CNS. Frontiers in Immunology. 2019;10:1928.

35. Mutso M, St John JA, Ling ZL, Burt FJ, Poo YS, Liu X, et al. Basic insights into Zika virus infection of neuroglial and brain endothelial cells. The Journal of General Virology. 2020 Jun;101(6):622–34.

36. Guzman-Martinez L, Maccioni RB, Andrade V, Navarrete LP, Pastor MG, Ramos-Escobar N. Neuroinflammation as a Common Feature of Neurodegenerative Disorders. Frontiers in Pharmacology. 2019;10:1008.

37. Zhang B-Z, Chu H, Han S, Shuai H, Deng J, Hu Y, et al. SARS-CoV-2 infects human neural progenitor cells and brain organoids. Cell Research. 2020 Aug 4;1–4.

38. Imai M, Iwatsuki-Horimoto K, Hatta M, Loeber S, Halfmann PJ, Nakajima N, et al. Syrian hamsters as a small animal model for SARS-CoV-2 infection and countermeasure development. Proc Natl Acad Sci U S A. 2020 14;117(28):16587–95.

39. Korber B, Fischer WM, Gnanakaran S, Yoon H, Theiler J, Abfalterer W, et al. Tracking Changes in SARS-CoV-2 Spike: Evidence that D614G Increases Infectivity of the COVID-19 Virus. Cell. 2020 Aug 20;182(4):812-827.e19.

40. Cornillez-Ty CT, Liao L, Yates JR, Kuhn P, Buchmeier MJ. Severe Acute Respiratory Syndrome Coronavirus Nonstructural Protein 2 Interacts with a

Host Protein Complex Involved in Mitochondrial Biogenesis and Intracellular Signaling. J Virol. 2009 Oct;83(19):10314–8.

41. Espíndola O de M, Siqueira M, Soares CN, Lima MASD de, Leite ACCB, Araujo AQC, et al. Patients with COVID-19 and neurological manifestations show undetectable SARS-CoV-2 RNA levels in the cerebrospinal fluid. International Journal of Infectious Diseases. 2020 Jul 1;96:567–9.

42. Crunfli F, Carregari VC, Veras FP, Vendramini PH, Valenca AGF, Antunes ASLM, et al. SARS-CoV-2 infects brain astrocytes of COVID-19 patients and impairs neuronal viability. medRxiv. 2020 Oct 13;2020.10.09.20207464.

43. Garcez PP, Nascimento JM, de Vasconcelos JM, Madeiro da Costa R, Delvecchio R, Trindade P, et al. Zika virus disrupts molecular fingerprinting of human neurospheres. Sci Rep. 2017 23;7:40780.

44. Pinto BGG, Oliveira AER, Singh Y, Jimenez L, Gonçalves ANA, Ogava RLT, et al. ACE2 Expression Is Increased in the Lungs of Patients With Comorbidities Associated With Severe COVID-19. J Infect Dis. 2020 Jul 23;222(4):556–63.

45. Annweiler C, Cao Z, Wu Y, Faucon E, Mouhat S, Kovacic H, et al. Counter-regulatory “Renin-Angiotensin” System-based Candidate Drugs to Treat COVID-19 Diseases in SARS-CoV-2-infected patients. Infect Disord Drug Targets. 2020 May 17;

46. Liu M, Wang T, Zhou Y, Zhao Y, Zhang Y, Li J. Potential Role of ACE2 in Coronavirus Disease 2019 (COVID-19) Prevention and Management. J Transl Int Med. 2020 May 9;8(1):9–19.

47. Rocha NP, Simoes E Silva AC, Prestes TRR, Feracin V, Machado CA, Ferreira RN, et al. RAS in the Central Nervous System: Potential Role in Neuropsychiatric Disorders. Curr Med Chem. 2018;25(28):3333–52.

48. Mazza MG, De Lorenzo R, Conte C, Poletti S, Vai B, Bollettini I, et al. Anxiety and depression in COVID-19 survivors: Role of inflammatory and

clinical predictors. Brain, Behavior, and Immunity [Internet]. 2020 Jul 30 [cited 2020 Aug 26]; Available from: http://www.sciencedirect.com/science/article/pii/S0889159120316068

49. Phan T. Genetic diversity and evolution of SARS-CoV-2. Infect Genet Evol. 2020 Jul;81:104260.

50. Weissman D, Alameh M-G, Silva T de, Collini P, Hornsby H, Brown R, et al. D614G Spike Mutation Increases SARS CoV-2 Susceptibility to Neutralization. medRxiv. 2020 Sep 12;2020.07.22.20159905.

51. Angeletti S, Benvenuto D, Bianchi M, Giovanetti M, Pascarella S, Ciccozzi M. COVID-2019: The role of the nsp2 and nsp3 in its pathogenesis. J Med Virol. 2020;92(6):584–8.

52. Rehman S, Mahmood T, Aziz E, Batool R. Identification of novel mutations in SARS-COV-2 isolates from Turkey. Arch Virol. 2020 Dec;165(12):2937–44.

53. Li Q, Wu J, Nie J, Zhang L, Hao H, Liu S, et al. The Impact of Mutations in SARS-CoV-2 Spike on Viral Infectivity and Antigenicity. Cell. 2020 Sep 3;182(5):1284-1294.e9.

54. Koyama T, Platt D, Parida L. Variant analysis of SARS-CoV-2 genomes. Bull World Health Organ. 2020 Jul 1;98(7):495–504.

55. Laamarti M, Alouane T, Kartti S, Chemao-Elfihri MW, Hakmi M, Essabbar A, et al. Large scale genomic analysis of 3067 SARS-CoV-2 genomes reveals a clonal geo-distribution and a rich genetic variations of hotspots mutations. bioRxiv. 2020 May 21;2020.05.03.074567.

56. Alouane T, Laamarti M, Essabbar A, Hakmi M, Bouricha EM, Chemao-Elfihri MW, et al. Genomic Diversity and Hotspot Mutations in 30,983 SARS-CoV-2 Genomes: Moving Toward a Universal Vaccine for the “Confined Virus”? Pathogens. 2020 Oct;9(10):829.

57. Ogando NS, Ferron F, Decroly E, Canard B, Posthuma CC, Snijder EJ. The Curious Case of the Nidovirus Exoribonuclease: Its Role in RNA Synthesis and Replication Fidelity. Front Microbiol. 2019;10:1813.

58. Bradley BT, Maioli H, Johnston R, Chaudhry I, Fink SL, Xu H, et al. Histopathology and ultrastructural findings of fatal COVID-19 infections in Washington State: a case series. Lancet. 2020;396(10247):320–32.

59. Mallapaty S. Mini organs reveal how the coronavirus ravages the body. Nature. 2020 Jun 22;583(7814):15–6.

60. Remmelink M, De Mendonça R, D'Haene N, De Clercq S, Verocq C, Lebrun L, et al. Unspecific post-mortem findings despite multiorgan viral spread in COVID-19 patients. Crit Care [Internet]. 2020 Aug 12 [cited 2020 Aug 26];24. Available from: https://www.ncbi.nlm.nih.gov/pmc/articles/PMC7422463/

61. Pellegrini M, Calzascia T, Toe JG, Preston SP, Lin AE, Elford AR, et al. IL-7 Engages Multiple Mechanisms to Overcome Chronic Viral Infection and Limit Organ Pathology. Cell. 2011 Feb 18;144(4):601–13.

62. Michaelson MD, Mehler MF, Xu H, Gross RE, Kessler JA. Interleukin-7 is trophic for embryonic neurons and is expressed in developing brain. Developmental Biology. 1996 Oct 10;179(1):251–63.

63. Araujo DM, Cotman CW. Trophic effects of interleukin-4, -7 and -8 on hippocampal neuronal cultures: potential involvement of glial-derived factors. Brain Research. 1993 Jan 8;600(1):49–55.

64. Figueiredo CP, Barros-Aragão FGQ, Neris RLS, Frost PS, Soares C, Souza INO, et al. Zika virus replicates in adult human brain tissue and impairs synapses and memory in mice. Nature Communications. 2019 05;10(1):3890.

65. McCoy MK, Tansey MG. TNF signaling inhibition in the CNS: implications for normal brain function and neurodegenerative disease. Journal of Neuroinflammation. 2008 Oct 17;5(1):45.

66. Probert L. TNF and its receptors in the CNS: The essential, the desirable and the deleterious effects. Neuroscience. 2015 Aug 27;302:2–22.

67. Singh AK, Bhushan B, Maurya A, Mishra G, Singh SK, Awasthi R. Novel coronavirus disease 2019 (COVID-19) and neurodegenerative disorders. Dermatologic Therapy. n/a(n/a):e13591.

68. Da Silveira Paulsen B, De Moraes Maciel R, Galina A, Da Silveira MS, Souza CDS, Drummond H, et al. Altered Oxygen Metabolism Associated to Neurogenesis of Induced Pluripotent Stem Cells Derived from a Schizophrenic Patient. Cell Transplant. 2012 Jul 1;21(7):1547–59.

69. Sochacki J, Devalle S, Reis M, Mattos P, Rehen S. Generation of urine iPS cell lines from patients with Attention Deficit Hyperactivity Disorder (ADHD) using a non-integrative method. Stem Cell Res. 2016;17(1):102–6.

70. Casas BS, Vitória G, do Costa MN, Madeiro da Costa R, Trindade P, Maciel R, et al. hiPSC-derived neural stem cells from patients with schizophrenia induce an impaired angiogenesis. Translational Psychiatry. 2018 Feb 22;8(1):1–15.

71. Cruvinel E, Ogusuku I, Cerioni R, Rodrigues S, Gonçalves J, Góes ME, et al. Long-term single-cell passaging of human iPSC fully supports pluripotency and high-efficient trilineage differentiation capacity. SAGE Open Med. 2020;8:2050312120966456.

72. Ramakers C, Ruijter JM, Deprez RHL, Moorman AFM. Assumption-free analysis of quantitative real-time polymerase chain reaction (PCR) data. Neurosci Lett. 2003 Mar 13;339(1):62–6.

73. Ruijter JM, Ramakers C, Hoogaars WMH, Karlen Y, Bakker O, van den Hoff MJB, et al. Amplification efficiency: linking baseline and bias in the analysis of quantitative PCR data. Nucleic Acids Res. 2009 Apr;37(6):e45.

74. Wölfel R, Corman VM, Guggemos W, Seilmaier M, Zange S, Müller MA, et al. Virological assessment of hospitalized patients with COVID-2019. Nature. 2020 May;581(7809):465–9.

75. Thompson JD, Higgins DG, Gibson TJ. CLUSTAL W: improving the sensitivity of progressive multiple sequence alignment through sequence weighting, position-specific gap penalties and weight matrix choice. Nucleic Acids Res. 1994 Nov 11;22(22):4673–80.

76. Kumar S, Stecher G, Li M, Knyaz C, Tamura K. MEGA X: Molecular Evolutionary Genetics Analysis across Computing Platforms. Mol Biol Evol. 2018 01;35(6):1547–9.

77. Jones DT, Taylor WR, Thornton JM. The rapid generation of mutation data matrices from protein sequences. Comput Appl Biosci. 1992 Jun;8(3):275–82.